

Disruption of a Proto-Planetary Disk by the Black Hole at the Milky Way Centre

Ruth A. Murray-Clay* & Abraham Loeb

Institute for Theory & Computation

Harvard-Smithsonian Center for Astrophysics

60 Garden Street, Cambridge, MA 02138, USA

Recently, an ionized cloud of gas was discovered plunging toward the supermassive black hole, SgrA*, at the centre of the Milky Way. The cloud is being tidally disrupted along its path to closest approach at ~ 3100 Schwarzschild radii from the black hole. Here, we show that the observed properties of this cloud of gas can naturally be produced by a proto-planetary disk surrounding a low-mass star, which was scattered from the observed ring of young stars orbiting SgrA*. As the young star approaches the black hole, its disk experiences both photo-evaporation and tidal disruption, producing a cloud. Our model implies that planets form in the Galactic centre, and that tidal debris from proto-planetary disks can flag low mass stars which are otherwise too faint to be detected.

Introduction

Observations of the galactic centre recently yielded a cloud of ionized gas and dust falling inward on a nearly radial orbit.¹ The cloud will reach pericenter in the summer of 2013, approaching our galaxy’s central black hole, SgrA*, at a distance of only 270 AU. As this plunge progresses, tidal gravity from the black hole will disrupt the infalling cloud, providing a unique probe of gas flow near SgrA*.

*rmurray-clay@cfa.harvard.edu

The apocenter of the cloud’s orbit, at $r_{\text{apo}} = 8400 \text{ AU} = 0.04 \text{ pc}$ from the black hole, coincides with the inner edge of the ring of young stars orbiting SgrA*, and the plane of the cloud’s orbit coincides with that of the ring.^{1,2} The ring’s age, estimated from its population of O/WR stars, is $\sim 4\text{--}8 \text{ Myr}$.³ At ages $\lesssim 3 \text{ Myr}$, most low mass stars host proto-planetary gas disks⁴ with radii of order 100 AU,⁵ and $\sim 1/5$ of stars with mass $0.1 - 1M_{\odot}$ retain their disks at ages of $\sim 5 \text{ Myr}$.^{6,7} Given the black hole mass of $M_{\text{BH}} = 4.3 \times 10^6 M_{\odot}$,^{8,9} the tidal radius around a star of mass m_{\star} at a distance $r = 0.04 \text{ pc}$ from SgrA* is $d_t \sim r(m_{\star}/3M_{\text{BH}})^{1/3} \sim 40 \text{ AU} (m_{\star}/M_{\odot})^{1/3}$. A solar mass star could therefore host a stable disk with a radius of $d_{\text{out}} \sim d_t/3 \sim 12 \text{ AU}$ on a roughly circular orbit near the inner edge of the young stellar ring. Similarly, an M-dwarf with mass $m_{\star} = 0.3M_{\odot}$ could host a stable disk having radius $d_{\text{out}} \sim 8 \text{ AU}$.

We suggest that the newly discovered gas cloud¹ surrounds such a star, which was scattered away from its original ring orbit and is currently plunging toward the supermassive black hole (Figure 1). The star itself is too low mass to be observable, but the debris produced through the disruption of its proto-planetary disk allowed it to be detected. We first calculate the properties of the system at the cloud’s observed location and argue that they match the observations—an ionized cloud $\sim 100 \text{ AU}$ in radius with density $n \sim 3 \times 10^5 \text{ cm}^{-3}$, an electron temperature of 10^4 K , and a dust temperature of $\sim 550 \text{ K}$, trailed by a stream of gas. We then provide predictions regarding the evolution of the cloud as it approaches pericenter. Finally, we demonstrate that the probability of producing such an object is plausibly high, and we calculate the implied rate of mass deposition by this process within the young stellar ring.

Results

Mass loss. Although the tidal radius for a solar-mass star at $r = 0.04 \text{ pc}$ is 40 AU , the tidal radius at the cloud’s pericenter distance of $r_p = 270 \text{ AU} = 10^{-3} \text{ pc}$ is only $d_t = 1 \text{ AU} (m_{\star}/M_{\odot})^{1/3}$. At the most recently observed epoch,¹ the cloud was approximately $6r_p$ from the black hole, with a tidal radius of $6 \text{ AU} (m_{\star}/M_{\odot})^{1/3}$. Hence, the circumstellar disk is

already experiencing substantial tidal disruption. At the same time, the Galactic centre hosts an extreme flux of ionizing and Far Ultraviolet (FUV) photons. Proto-planetary disks in the ionizing environment near O stars in the Trapezium cluster are known to experience photoevaporation.¹⁰ The stars experience mass loss due to heating both by FUV and by Lyman limit photons.¹¹ The former heat the disk to $\sim 10^3$ K, generating outflows at the sound speed of ~ 3 km s $^{-1}$, corresponding to the escape velocity at a distance ~ 100 AU (m_*/M_\odot) from the star. Well within this distance, the FUV-driven outflow is diminished, though not entirely quenched.¹² At the ~ 10 AU and smaller distances of interest here and given the extreme ionizing environment, Lyman continuum (ionizing) photons dominate the outflow, generating a $\sim 10^4$ K ionized outflow moving at the sound speed of ~ 10 km s $^{-1}$. This speed matches the escape velocity at a distance of $d_{\text{esc}} \sim 10$ AU (m_*/M_\odot) from the star. Loss from smaller distances occurs at a reduced rate, but still generates a ~ 10 km s $^{-1}$ outflow by the time the gas reaches d_{esc} .

Which process—tidal stripping or photoevaporation—dominates mass loss from the disk? Currently, tidal stripping dominates the unbinding of mass from the star, and at large distances from the star tidal stripping determines the ultimate fate of the gas. However, the outflow properties of the observed cloud are nevertheless currently determined by photoevaporation. This can be understood as follows. Gas at a distance $d > d_t$ from its host star is accelerated by the tidal potential to a relative speed of Δv as it moves of order its own radius away from its host star: $\Delta v \sim (GM_{\text{BH}}/r^2)(d/r)(d/\Delta v)$, so that $\Delta v \sim v_{\text{circ}}(d/r)$, with $v_{\text{circ}} = (GM_{\text{BH}}/r)^{1/2}$. For $d = d_t$, $\Delta v \sim v_{\text{circ}}(m_*/M_{\text{BH}})^{1/3}$. At the cloud’s current separation from SgrA*, $r \approx 6 \times 10^{-3}$ pc ≈ 1300 AU, $v_{\text{circ}} \approx 1700$ km s $^{-1}$ and $\Delta v \sim 10$ km s $^{-1}(m_*/M_\odot)^{1/3}$ at the tidal radius, comparable to the wind outflow rate. Hence, the motion of tidally decoupled gas is dominated by the tidal field. At earlier times in the star’s plunge, Δv was smaller, meaning that wind gas flowed out of the tidal radius faster than tidally disrupted gas. Currently, near the disk edge, the dynamics of previously ejected gas are set by properties of the wind, while on the ~ 100 AU scale of the cloud, tidal evolution overwhelms wind motions.

Although the current mass disruption rate of the proto-planetary disk, \dot{M}_{dis} , is larger than the wind outflow rate, \dot{M}_w , wind gas emitted at earlier times dominates the currently observed cloud. In the short time that the infalling star has spent in an enhanced tidal field with $d_t < d_{\text{out}}$, the disk has only had the opportunity to expand by a fraction of its ~ 10 AU size. At $d = 8$ AU, the time since $d_t = d$ along the infalling star's orbit is $\Delta t = 3$ yr for $m_* = 0.3 M_\odot$. Decoupled material has traveled only $\sim \Delta v \Delta t \sim 4$ AU further from the host star in that time. Figure 2 illustrates this point. We ask how far a test particle, released at a given disk radius, d , from the star when $d_t = d$ and moving only under the gravity of the black hole, will be from its current orbit. Exterior to the decoupled material, gas originally launched in a wind dominates.

The tidal decoupling rate in the disk is $\dot{M}_{\text{dis}} \sim 2\pi \Sigma d_t \dot{d}_t \sim 2\pi \Sigma d_t \dot{r} (m_*/3M_{\text{BH}})^{1/3}$, where $\Sigma(d)$ is the original surface density of the disk and $\dot{r} \approx 2000$ km s $^{-1}$ at the current position in the cloud's orbit. For illustration, we choose a profile similar to the minimum-mass solar nebula: $\Sigma = \Sigma_0 (d/d_0)^{-1}$ with $\Sigma_0 = 2 \times 10^3$ g cm 2 and $d_0 = 1$ AU.⁵ This choice yields a current $\dot{M}_{\text{dis}} \sim 3 \times 10^{-3} M_\odot \text{ yr}^{-1} (m_*/M_\odot)^{1/3}$, where we set d equal to the current tidal radius. Photoevaporation, on the other hand, gives mass loss rates^{13,14} of $\dot{M}_w \sim 3 \times 10^{-10} (d_{\text{out}}/10 \text{ AU})^{3/2} (\Phi_{i,49}/D_{\text{pc}}^2)^{1/2} M_\odot \text{ yr}^{-1}$ for disks with sizes $d_{\text{out}} > d_{\text{esc}}$, where $\Phi_{i,49}$ is the ionizing luminosity, Φ_i , in units of 10^{49} s $^{-1}$ of a source at distance D from the disk, with $D_{\text{pc}} = D/(1 \text{ pc})$.

The photoevaporation mass loss can be derived as follows. At $d = d_{\text{esc}}$, the escape velocity is comparable to the wind's sound speed $c_s = 10$ km s $^{-1}$. For $d \gtrsim d_{\text{esc}}$, $\dot{M}_w \approx 4\pi d^2 m_p n_b c_s$, where m_p is the mass of a proton and we have neglected an order unity correction arising from the non-sphericity of the flow. We refer to the surface layer of the disk within which photoionization heats disk gas to $\sim 10^4$ K as the “base of the wind.” At the base of the wind, a balance between photoionization and radiative recombination yields a number density of $n_b \sim (\Phi_i/4\pi D^2)^{1/2} (\alpha_{\text{rec}} d)^{-1/2}$, where $\alpha_{\text{rec}} = 2.6 \times 10^{-13} \text{ cm}^3 \text{ s}^{-1}$ is the Case B radiative recombination coefficient for hydrogen at a temperature of

10^4 K, and we have used the fact that the optical depth to ionizing photons is unity. Hence, $\dot{M} \sim (4\pi/\alpha_{\text{rec}})^{1/2} m_p c_s d^{3/2} (\Phi_i/D^2)^{1/2}$. Though this expression is only good to order of magnitude, its coefficient is in fortuitously good agreement with more detailed wind models.^{13,14} Observations yield $10^{50.8} \text{ s}^{-1}$ Lyman continuum photons in the central parsec^{1,15}, corresponding to $\Phi_{i,49} = 63$. Using $D = 1\text{pc}$, $(\Phi_{i,49}/D_{\text{pc}}^2)^{1/2} = 8$. The central concentration of S-stars within 0.01 pc, which we estimate to contribute $\Phi_{i,49} = 0.2$ from each of ten approximately $10M_\odot$ stars comparable to the second-most luminous Trapezium star,¹³ yields a small total of $\Phi_{i,49} = 2$ but in a more concentrated region. At the current position of the cloud, these stars contribute $(\Phi_{i,49}/D_{\text{pc}}^2)^{1/2} \sim 230$ for $D = 6 \times 10^{-3}\text{pc}$. At $D = 0.04\text{pc}$, this number is 35. For $d = 10\text{AU}$ and smaller, mass loss from these ionizing fluxes dominates over FUV-driven mass loss. Using an intermediate value of $(\Phi_{i,49}/D_{\text{pc}}^2)^{1/2} = 100$, $\dot{M}_w \sim 3 \times 10^{-8} M_\odot \text{ yr}^{-1} (d_{\text{out}}/10\text{AU})^{3/2}$. On the cloud's original orbit, $\dot{M}_w \sim 10^{-8} M_\odot \text{ yr}^{-1} (d_{\text{out}}/10\text{AU})^{3/2}$, allowing our nominal disk, which contains $\sim 10^{-2} M_\odot$ between 1 and 8 AU, to survive for $\sim 10^6$ yr. Disk masses several times larger are plausible, and hence a proto-planetary disk could have survived until the current time on the star's birth orbit in the ring.

Dynamics of stripped gas. Currently, gas farther than ~ 12 AU from the star (for $m_* = 0.3M_\odot$; see Figure 2) was originally ejected in the photoevaporative wind. This ejected material (which starts in a ring-like configuration) itself undergoes tidal stripping. Along the star's original orbit, the extent of the wind moving at $\sim 10 \text{ km s}^{-1}$ is set by the original 24 AU tidal radius. Since gas requires only 10 years to travel 24 AU at 10 km s^{-1} , this wind scale applies even if the wind region was disrupted by close stellar encounters or more distant encounters with the black hole at some point in the past.

As the star plunges toward the Galactic centre, its disk and wind are pulled off in shells as the tidal radius shrinks (Figure 3). The time for a parcel of wind to travel at 10 km s^{-1} from 10 to 100 AU is comparable to the 70 year time to plunge to pericenter on the cloud's current orbit. This wind-generated cloud in turn experiences tidal disruption.

By its current location, the original wind cloud will have reached an extent of a few hundred AU. Figure 2 illustrates this extent for $m_* = 0.3M_\odot$. We note that although previous close encounters with the black hole may have stripped the disk to smaller than its original size, the disk wind is regenerated over each orbit. As long as the disk size exceeds d_{esc} and most of the disk mass remains intact, our wind calculation remains valid. If the disk is stripped to smaller sizes, a wind will still be blown, but with reduced \dot{M}_w .

Ram pressure of the ambient gas exceeds the ram pressure of the photoevaporative wind when $n_{\text{amb}}v_*^2 > nv_w^2$, where n_{amb} is the ambient number density of gas and v_* is the star's velocity along its orbit. The characteristic density of ambient gas within the central 1.5pc is $n_{\text{amb}} \sim 10^3 \text{ cm}^{-3}$.²⁰ Models place the density at $\sim 3 \times 10^2$ – $6 \times 10^3 \text{ cm}^{-3}$ at the cloud's current location and $\sim (1\text{--}5) \times 10^2 \text{ cm}^{-3}$ on its original orbit.¹⁶ Along the star's original orbit, $v_* \approx 700 \text{ km s}^{-1}$, and the ram pressure force from the disk wind roughly balances ram pressure with the ambient medium at the star's tidal radius. Currently, $v_* \approx 2300 \text{ km s}^{-1}$, so ram pressure with the surrounding medium has increased by 1–2 orders of magnitude at comparable separations from the star, and the tidally-disrupted photoevaporative wind is undergoing ram pressure stripping. Nevertheless, at the current tidal radius, the two pressures remain in rough balance and our estimates of the mass loss rate are therefore valid. As the cloud continues its plunge toward the super-massive black hole, its outer (tidally detached) extent will be shaped by ram pressure stripping.

Figure 4a displays the inferred ionized density of the cloud as a function of radial scale. From the total Br γ line luminosity, the discovery paper¹ calculates an electron density of $2.6 \times 10^5(d/125\text{AU})^{-3/2}$, in excellent agreement with our prediction. In Figure 4a, we also plot the contribution to the total line luminosity as a function of radial scale. Since the luminosity is proportional to n^2d^3 , this contribution peaks at the outer edge of the disk, but the contribution from the extended cloud falls off slowly, as $1/d$, so that about 1/5 of the line luminosity comes from 100 AU scales. We note that though the majority of Br γ emission comes from the 10–20 AU scale of the tidally expanded disk, the majority of the

mass in the cloud is at large scales since the cloud mass is proportional to $nd^3 \propto d$. At these large scales, full hydrodynamic simulations including ram pressure stripping and tidal gravity in 3D are required to match in detail the surface brightness, shape, and velocity width of the observed emission. One might naively expect the surface of the cloud to be Kelvin-Helmholtz unstable.¹ However, observations of cold fronts in X-ray clusters indicate that gas clouds moving at a Mach number of order unity through a hot (\sim keV) ambient medium maintain a smooth surface, probably due to "magnetic draping".¹⁷

Discussion

We predict (Figure 4b) that the total Br γ luminosity of the cloud will increase as it approaches pericenter. This future evolution of a debris cloud around a low-mass star on a Keplerian orbit is easily distinguishable from that of a pressure-confined cloud with no self gravity or central mass supply. We further predict that with better resolution, the specific intensity of the line should increase since most of the emission is coming from a smaller spread in velocities than is currently resolved.

The dust in the wind, in analogy to dust in HII regions, does not reach temperature equilibrium with the 10^4 K gas. Gillessen et al. argue that the dust continuum emission at about 550 K comes from small, transiently heated grains, having a total mass equal to $\sim 10^{-5}$ the total gas mass of the cloud.¹ Additional colder dust may be present. This relatively small dust mass may result from grain growth and settling in the proto-planetary disk, leaving relatively few small grains available to be lofted into the photoevaporative wind. The neutral, cooler disk does not contribute substantially to the observed dust emission.

As demonstrated above, a $\sim 3 \times 10^{-2} M_\odot$ disk can survive on the star's original orbit for ~ 3 Myr. In the Supplementary Discussion, we discuss the likely rate at which such disks could be scattered onto orbits comparable to the observed gas cloud. This rate primarily depends on the highest mass scatterers in the ring of young stars around SgrA*. It could increase considerably above a minimum value 0.1% if the stellar mass function extends above

the observed $60M_{\odot}$ limit (as observed elsewhere in the Galaxy), if there are intermediate mass black holes¹⁸ of 10^2 – 10^3M_{\odot} , or if compact star clusters (such as the observed clusters IRS 13N or IRS 13E) act as massive scatterers. Finally, if a $0.03 M_{\odot}$ disk is disrupted by the black hole every $\sim 5 \times 10^5$ yr, the related events deliver $\sim 6 \times 10^{-8}M_{\odot}$ yr⁻¹ to the inner 0.01 pc around SgrA*, comparable to the presently inferred accretion rate onto the black hole.¹⁹

We note that alternative explanations invoking mass loss during rare evolutionary phases of stars (such as a proto-planetary nebula around an emerging white dwarf or a debris envelope around a merged blue straggler), have a much lower probability of occurrence than our scenario. They share the requirement for a rare kick, but involve progenitors which are much less abundant than low-mass stars in the ring of young stars around SgrA*.

The existence of proto-planetary disks in galactic nuclei has important implications: it could lead to a fragmentation cascade to comets, asteroids, and dust around quasars,²⁰ and to bright flares due to the tidal disruption of planets,²¹ as well as transits of hypervelocity stars.²² In the Milky Way centre, the debris of proto-planetary disks offers a new probe of the low mass end of the mass distribution of stars which are too faint to be detected otherwise.

Acknowledgements. We thank Andi Burkert, Reinhard Genzel, and Chris McKee for stimulating discussions. AL was supported in part by NSF grant AST-0907890 and NASA grants NNX08AL43G and NNA09DB30A.

Author contributions. Both authors originated the idea for the project and worked out collaboratively its general details. R.M.C. performed the N-body simulation described in the Supplementary Discussion.

Competing Financial Interests: The authors have no competing financial interests.

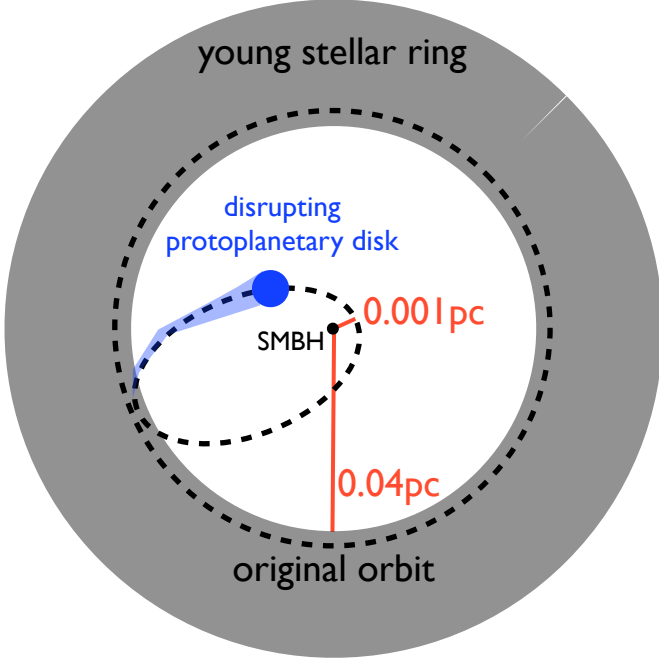


Figure 1: Proto-planetary disk plunging toward the galactic centre. Schematic illustration of our scenario. A young, low-mass star hosting a proto-planetary disk is dynamically dislodged from its original orbit (dashed circle) in the Galactic centre’s young stellar ring (gray). As it plunges toward the supermassive black hole (SMBH) at the Galactic centre (orbit indicated by dashed ellipse), the disk is photoevaporated and tidally disrupted, generating an extended dusty cloud around the star (blue circle). A trail of dust and gas is deposited along the star’s orbit (extended blue trail).

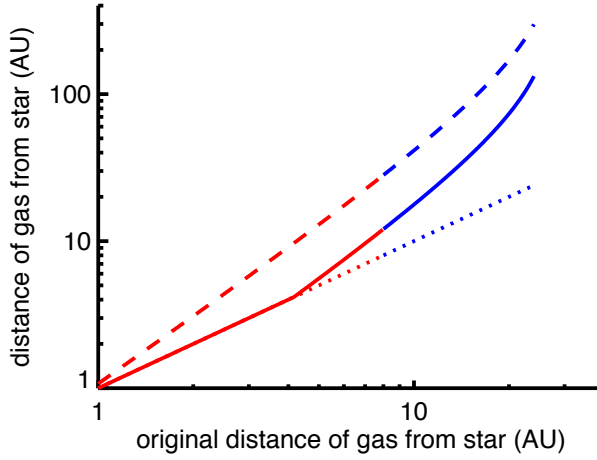


Figure 2: Expansion of the infalling gas. As the star plunges toward the Galactic centre, its disk and the surrounding photoevaporative wind are tidally disrupted. For a fiducial stellar mass of $m_* = 0.3M_\odot$, we plot the distance, d , of gas from the host star at the current epoch (solid line) and at the time of pericenter passage (dashed line) as a function of separation from the host star at the time of tidal decoupling. The dotted line represents no change. We assume that the material is instantaneously decoupled from the star when its separation equals the tidal radius and that it subsequently moves as a test particle in the gravitational field of the supermassive black hole. At the time of its decoupling, the test particle is started with the orbital parameters that the cloud had at time d/v_* prior to decoupling, and the full separation between the test particle and the star is thereafter calculated as a function of time. Red portions of the curve represent gas initially in the disk, while blue portions represent gas initially in the photoevaporative cloud. For gas currently observed in the cloud, the tidal evolution depicted here dominates the wind structure at large scales, while the wind outflow at $\sim 10 \text{ km s}^{-1}$ dominates the structure of recently ejected gas near the disk rim. At pericenter, tidal evolution determines the structure of the entire wind.

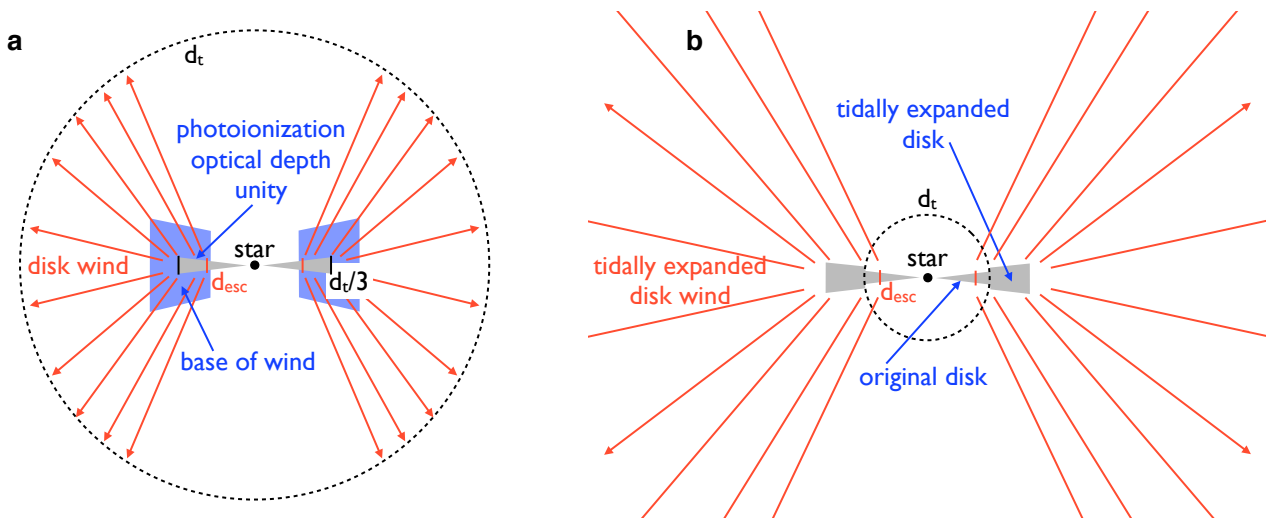


Figure 3: Disk and wind structure. Schematic diagram of the disk and wind structure on the star's original orbit in the young stellar ring (**a**) and at the current epoch (**b**). On its original orbit, the star (black circle) hosts a protoplanetary disk (gray), which is limited in extent (vertical black line) to approximately one third of the star's tidal radius, d_t (dashed circle). Photoionization efficiently launches a wind beyond d_{esc} , where gas is heated enough that its thermal velocity is comparable to the stellar escape velocity (vertical red line). From the wind launching region (blue), gas flows outward (red arrows) until it passes the tidal radius and is stripped from the star. At the current epoch, d_t has shrunk, causing both the disk and the wind to tidally expand.

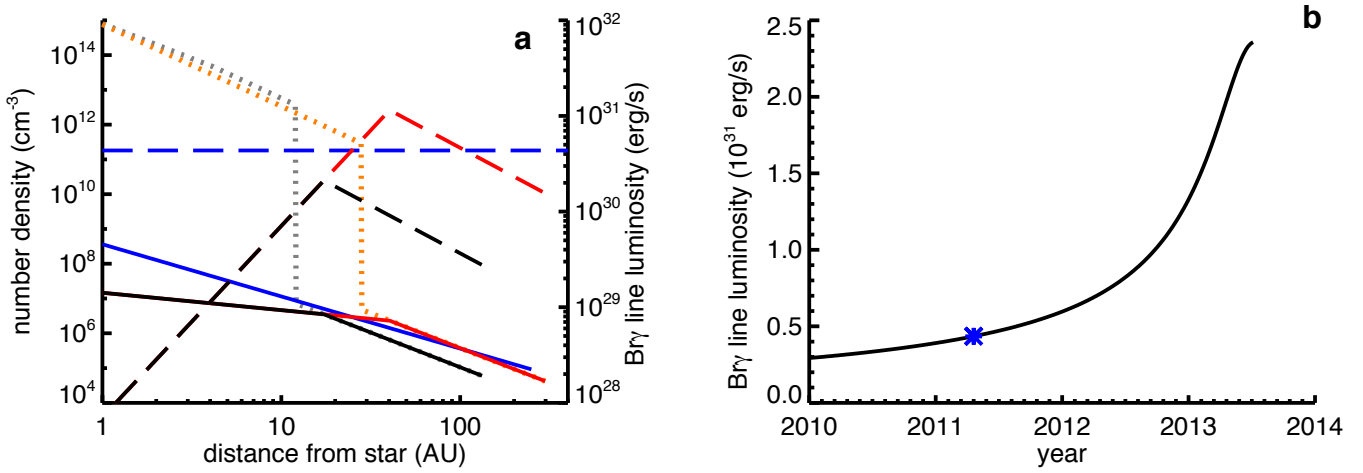


Figure 4: Observational predictions. Ionized gas in the disk wind generates $\text{Br}\gamma$ line luminosities in good agreement with observations. (a), left axis: The cloud’s ionized gas number density is inferred from the observed $\text{Br}\gamma$ line luminosity to be¹ $2.6 \times 10^5 (d/125\text{AU})^{-3/2} \text{ cm}^{-3}$ for emission dominated by gas at a distance d from the center of the cloud (blue, solid). We approximate the neutral number density in the disk as $n = m_p^{-1} \Sigma_0 (d_i/d_0)^{-1} h_d^{-1} (d_i/d)^2$, where d_i is the initial separation of the gas from the host star and we use a disk scale-height $h_d \sim 0.1d$. We show the ionized density, n_+ at the current epoch (black, solid) and at the time of pericenter passage (red, solid) for $m_* = 0.3M_\odot$. Where wind gas dominates, we estimate $n_+ = \dot{M}_w (2\pi m_p d^2 v_w)^{-1}$ with $\dot{M}_w = 3 \times 10^{-8} (d_{\text{out}}/10\text{AU})^{3/2} M_\odot/\text{yr}$, assuming that the wind geometry is not yet spherically symmetric. We choose d_{out} to be the current outer limit of the tidally disrupting disk. This estimate is not good at the largest separations, where tidal evolution and ram pressure stripping modify the gas density (see text). Where the disk itself is present, the neutral gas number density in the disk (gray dotted, current; orange dotted, pericenter) is 5–8 orders of magnitude larger than the ionized number density at the disk surface. We therefore set $n_+ = n_b$, the number density at the base of the ionized wind (see text). Near the outer edge of the disk, the observed number density is in excellent agreement with the modeled density, given the approximate nature of this model. (a), right axis: $\text{Br}\gamma$ luminosity as a function of distance, d , from the infalling star, calculated using $L_{\text{Br}\gamma} = 2.35 \times 10^{-27} n_+^2 (4/3)\pi d^3$ (in c.g.s. units) now (black, dashed) and at pericenter (red, dashed) for the same model. The currently measured line luminosity is included for reference (blue, dashed), and is in good agreement with the model. Most of the total integrated line emission is coming from near the current disk edge at 10–20 AU, but $\sim 1/5$ of the emission comes from ~ 100 AU scales. (b) Total $\text{Br}\gamma$ line luminosity integrated over our model disk plus wind as a function of time, calculated as $L_{\text{Br}\gamma} = 2.35 \times 10^{-27} \times 2\pi \int n_+^2 d^2 dd$ (in c.g.s. units; using 2π to adjust for a non-spherical wind). We predict that the total line luminosity will increase by approximately a factor of 5 from its reported value (blue asterisk) as the star approaches pericenter in 2013.

REFERENCES

- 1.Gillessen, S. *et al.*, A Gas Cloud on Its Way Towards the Supermassive Black Hole in the Galactic Centre, *Nature* **481**, 51-54 (2012).
- 2.Bartko, H. *et al.*, Evidence for Warped Disks of Young Stars in the Galactic Center, *Astrophys. J.* **697**, 1741-1763 (2009).
- 3.Paumard, T. *et al.*, The Two Young Star Disks in the Central Parsec of the Galaxy: Properties, Dynamics, and Formation, *Astrophys. J.* **643**, 1011-1035 (2006).
- 4.Haisch, K.E., Lada, E.A., & Lada, C.J., Disk Frequencies and Lifetimes in Young Clusters, *Astrophys. J.* **553**, L153-L156 (2001).
- 5.Andrews, S.M. *et al.*, Protoplanetary Disk Structures in Ophiuchus, *Astrophys. J.* **700**, 1502-1523 (2009).
- 6.Carpenter, J.M., Mamajek, E.E., Hillenbrand, L.A., & Meyer, M.R., Evidence for Mass-Dependent Circumstellar Disk Evolution in the 5 Myr old Upper Scorpius OB Association, *Astrophys. J.* **651**, L49-L52 (2006).
- 7.Dahm, S.E. & Hillenbrand, L.A., Spitzer Observations of NGC 2362: Primordial Disks at 5 Myr, *Astrophys. J.* **133**, 2072-2086 (2007).
- 8.Gillessen, S. *et al.*, The Orbit of the Star S2 Around SGR A* from Very Large Telescope and Keck Data, *Astrophys. J.* **707**, L114-L117 (2009).
- 9.Ghez, A. *et al.*, Measuring Distance and Properties of the Milky Way's Central Supermassive Black Hole with Stellar Orbits, *Astrophys. J.* **689**, 1044-1062 (2008).
- 10.O'Dell, C.R., Wen, Z., & Hu, X., Discovery of New Objects in the Orion Nebula on HST Images - Shocks, Compact Sources, and Protoplanetary Disks, *Astrophys. J.* **410**, 696-700 (1993).
- 11.Störzer, H. & Hollenbach, D., Photodissociation Region Models of Photoevaporating Circumstellar Disks and Application to the Proplyds in Orion, *Astrophys. J.* **515** 669-684 (1999).

12.Adams, F.C. *et al.*, Photoevaporation of Circumstellar Disks Due to External Far-Ultraviolet Radiation in Stellar Aggregates, *Astrophys. J.* **611** 360-379 (2004).

13.Scally, A. & Clarke, C., Destruction of Protoplanetary Discs in the Orion Nebula Cluster, *MNRAS* **325**, 449-456 (2001).

14.Hollenbach, D., Yorke, H.W., & Johnstone, D., Disk Dispersal Around Young Stars, in Mannings, V., Boss, A.P., & Russell, S.S., eds, *Protostars and Planets IV*, Univ. Arizona Press, Tucson, AZ (2000).

15.Genzel, R., Eisenhauer, F., & Gillessen, S., The Galactic Center Massive Black Hole and Nuclear Star Cluster, *Rev. Mod. Phys.* **82**. 3121-3195 (2010).

16.Narayan, R., & McClintock, J. E., Advection-Dominated Accretion and the Black Hole Event Horizon, *New Astronomy Reviews* **51**, 733-751 (2008).

17.Markevitch, M., & Vikhlinin, A., Shocks and cold fronts in galaxy clusters, *Physics Reports* **443**, 1-53 (2007).

18.Gualandris, A., & Merritt, D., Perturbations of Intermediate-mass Black Holes on Stellar Orbits in the Galactic Center, *Astrophys. J.* **705**, 361-371 (2009).

19.Cuadra, J. *et al.*, Galactic Centre Stellar Winds and Sgr A* Accretion, *Mon. Not. R. Astron. Soc.* **366**, 358-372 (2006).

20.Nayakshin, S., Sazonov, S.,& Sunyaev, R., Are Supermassive Black Holes Shrouded by 'Super-Oort' Clouds of Comets and Asteroids?, *Mon. Not. R. Astron. Soc.* **419**, 1238-1247 (2011).

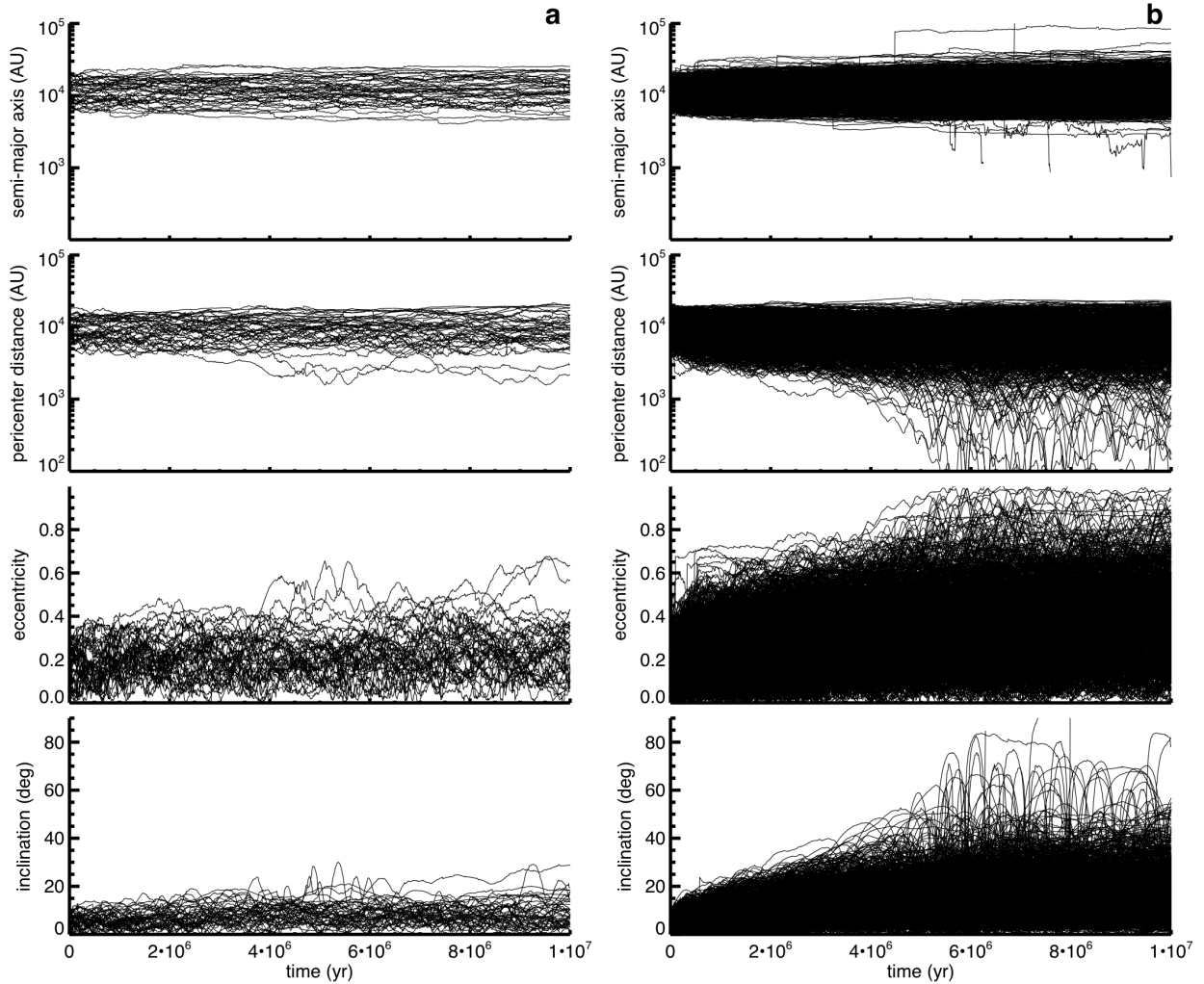
21.Zubovas, K., Nayakshin, S., & Markoff, S., Sgr A* Flares: Tidal Disruption of Asteroids and Planets?, *Mon. Not. R. Astron. Soc.* **421**, 1315-1324 (2012).

22.Ginsburg, I., Loeb, A., & Wegner, G. A., Hypervelocity Planets and Transits Around Hypervelocity Stars, *Mon. Not. R. Astron. Soc.* **423**, 948 (2012).

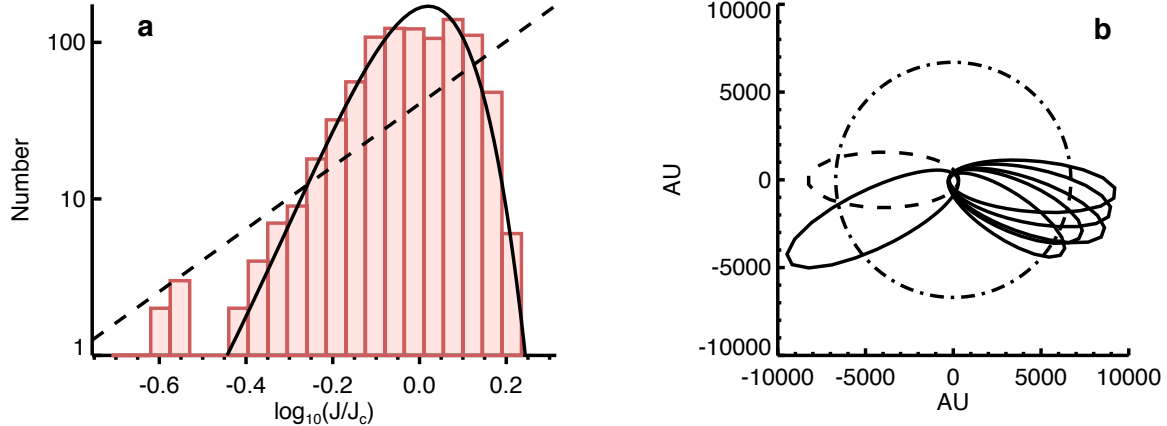
SUPPLEMENTARY INFORMATION
for “Disruption of a Proto-Planetary Disk by the
Black Hole at the Milky Way Centre”

Ruth A. Murray-Clay & Abraham Loeb

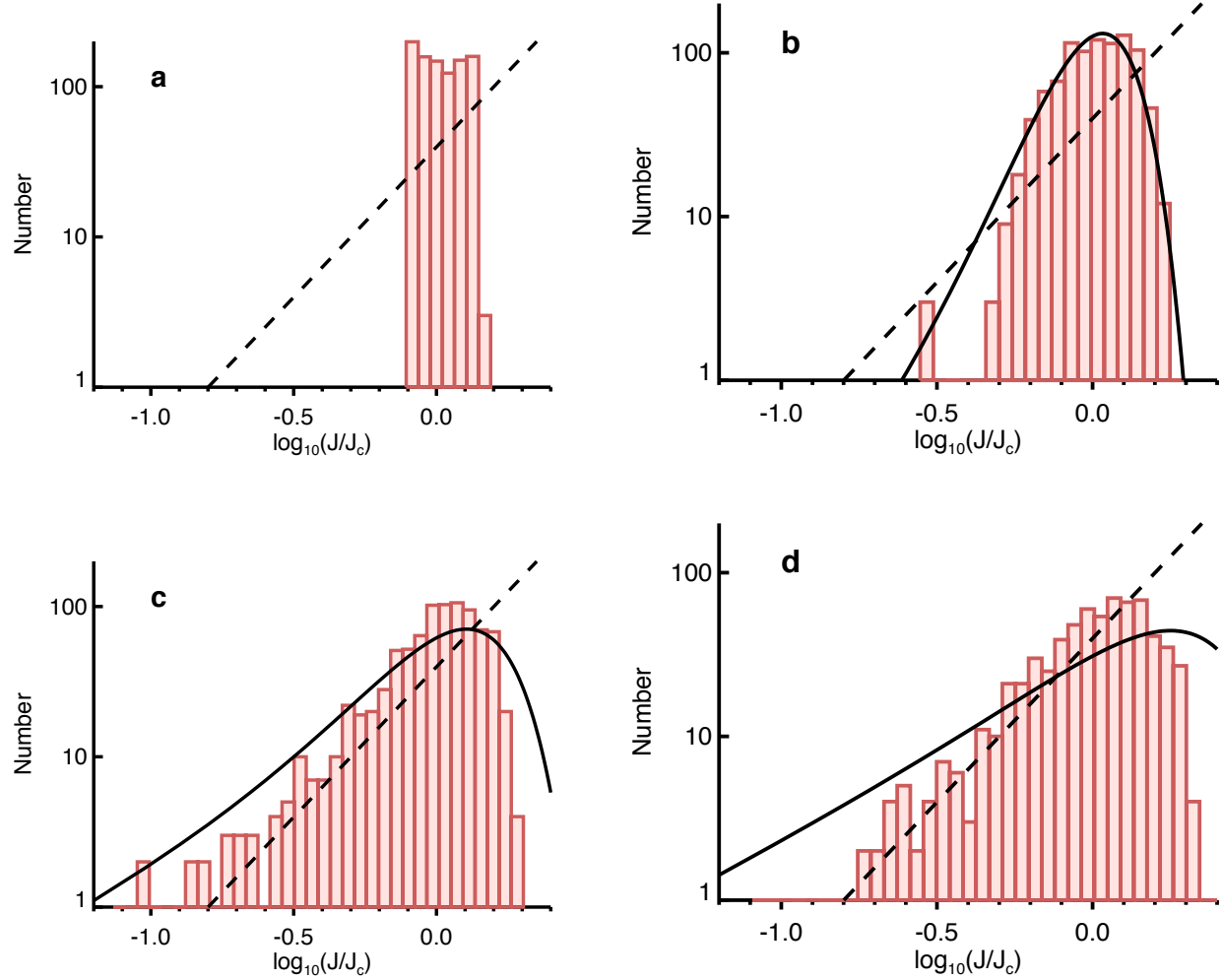
Supplementary Figures



Supplementary Figure S1: Dynamical properties of stars. Semi-major axes, pericenter distances, eccentricities, and inclinations for perturbing stars ($m_* = 60M_\odot$; **a**) and low-mass stars (test particles; **b**) as functions of time for our first simulation, described in the text. The perturbers maintain properties consistent with the young stellar ring, while a subset of low mass stars are delivered onto low angular momentum orbits.



Supplementary Figure S2: Results from N-body simulations. (a) Histogram of angular momenta of low mass stars at time 6×10^6 years for the same simulation shown in Figure 5. The number of stars is well matched by 1-D angular momentum diffusion (equation S5; solid). The expectation for a relaxed system, $N = N_*(J/J_c)^2\Delta$ (dashed), is plotted for reference. For the observed cloud, $\log_{10}(J/J_c) = -0.6$. (b) Orbits of simulated stars (solid) that reach pericenter distances smaller than that of the observed cloud (dashed) in less than 6×10^6 years. The inner edge of the young stellar ring is plotted for reference (dot dashed).



Supplementary Figure S3: Angular momenta of low mass stars. We show histograms at times 0 (**a**), 6×10^6 yr (**b**), 2.5×10^7 yr (**c**), and 10^8 yr (**d**) in a simulation containing 24 perturbers, each with $m_* = 100M_\odot$ (see text). The low-mass stellar population, which starts with evenly distributed angular momenta in the inner ring, is first matched by the 1D diffusion equation (Eq. 5; solid) and then by $N = N_*(J/J_c)^2 \Delta$ (dashed).

Supplementary Discussion

Scattering Probability. Proto-planetary disks hosted by young stars could be stripped by several possible mechanisms. In the main text, we have shown that on their initial orbits in the young stellar ring, such disks are not depleted by mass loss in disk winds over their several million year lifetimes. However, the same dynamical processes that could send a young star plunging toward the Galactic centre could themselves lead to disk stripping. In particular, scattering events can strip disks and, if the star’s orbital evolution is too gradual, earlier encounters with the central black hole could also produce stripping. To arrive on its current plunging orbit without losing its proto-planetary disk, a young star must: *(i)* experience sufficient orbital evolution over its lifetime due to scattering interactions at all distances to be placed on a highly eccentric orbit while avoiding single encounters that strip the disk, and then *(ii)* experience a final, strong encounter that substantially alters the star’s pericenter distance, again without stripping its disk. Requirement *(ii)* is needed so that the disk’s extent was not already truncated by tidal stripping at a comparable pericenter location during a previous plunge toward the black hole.

We note that disk winds can be driven by photoionization even if the disk is truncated at closer distances to the host star than those estimated above, so requirement *(ii)* is not strictly needed for our model. However, if requirement *(ii)* is not satisfied, the mass loss rate in the disk’s wind and hence the observed cloud density will be lower than estimated in the main text.

In order to investigate these requirements, we first consider the stripping potential of a single scattering encounter. We demonstrate that a final, strong encounter with a high mass star or intermediate mass black hole¹⁸ can change the pericenter distance of a plunging star without stripping its proto-planetary disk. We then show that, given choices about the distribution of massive perturbers that are consistent with observations, evolution of a low-mass star to a highly eccentric orbit followed by a strong final encounter could happen with reasonably high probability, all without disk stripping.

A single scattering encounter with a perturber of mass m_{pert} at impact parameter b and with relative velocity at infinity v_{enc} changes a star's velocity by $\Delta v_* \sim (Gm_{\text{pert}}/b^2)(2b/v_{\text{enc}})$. A given change in velocity Δv_* hence requires an impact parameter $b \sim 2Gm_{\text{pert}}/(v_{\text{enc}}\Delta v_*)$. Such an encounter tidally strips disk gas at radii r_d where the induced relative velocity between the star and its orbiting material, $\Delta v_{\text{tid}} \sim (Gm_{\text{pert}}/b^2)(2r_d/b)(2b/v_{\text{enc}})$ exceeds the star's escape velocity $v_{\text{esc},*} = (2Gm_*/r_d)^{1/2}$. Note that because we will be interested in $\Delta v_* \leq v_{\text{enc}}$, we can ignore gravitational focusing in our estimate of Δv_{tid} (encounters are not parabolic, as is often assumed in calculations of disk stripping during close stellar passages). During an encounter that changes the stellar velocity by Δv_* , the disk is stripped at radii $r_d \gtrsim (b/2)(v_{\text{esc},*}/\Delta v_*)$, or in other words, where $v_{\text{esc},*}^3 \lesssim 2(m_*/m_{\text{pert}})v_{\text{enc}}(\Delta v_*)^2$. We choose to express the location of stripping in terms of $v_{\text{esc},*}$ rather than r_d because disk winds are launched where the thermal velocity, v_{th} , of gas with temperature $T \sim 10^4 \text{ K}$ is comparable to the escape velocity from the star. The location, r_d , of this equality varies as a function of stellar mass. The change in stellar velocity generated by an encounter that does *not* strip gas at the disk radius with a given $v_{\text{esc},*}$ is limited to

$$\Delta v_* \lesssim \left(\frac{m_{\text{pert}}}{m_*} \frac{v_{\text{esc},*}^3}{2v_{\text{enc}}} \right)^{1/2} \quad (S1)$$

We may now estimate the perturber mass required to change a plunging star's pericenter distance by of order itself without truncating the star's disk at the radius corresponding to $v_{\text{esc},*} = v_{\text{th}}$. Since the star's orbit has an eccentricity of¹ $e = 0.938 \sim 1$, the specific angular momentum of its orbit around the black hole is approximately $J \approx (2GM_{\text{BH}}r_p)^{1/2}$, where r_p is the pericenter distance. A change in the star's orbital angular momentum of ΔJ corresponds to a change in pericenter distance $\Delta r_p \approx 2r_p(\Delta J/J)$. To generate $\Delta r_p = r_p/2$, a single scattering event at apocenter must change the star's apocenter velocity, $v_{\text{apo}} = [GM_{\text{BH}}(1 - e)/r_{\text{apo}}]^{1/2}$, by $\Delta v_{\text{apo}} \approx v_{\text{apo}}/4$. The cloud's current, post-scattering, apocenter velocity of $v_{\text{apo,f}} = (3/4)v_{\text{apo}} = 170 \text{ km s}^{-1}$ requires $\Delta v_* = \Delta v_{\text{apo}} = v_{\text{apo,f}}/3$.

A single scattering encounter near the apocenter of the star's orbit around the black hole can therefore generate $\Delta r_p = r_p/2$ without stripping the star's disk at the distance

corresponding to $v_{\text{esc},*} = v_{\text{th}}$ as long as the perturber has mass

$$\begin{aligned} m_{\text{pert}} &\gtrsim \frac{2}{9} m_* \frac{v_{\text{enc}} v_{\text{apo,f}}^2}{v_{\text{th}}^3} & (S2) \\ &\sim 100 M_\odot \left(\frac{m_*}{0.3 M_\odot} \right) \left(\frac{v_{\text{enc}}}{300 \text{ km s}^{-1}} \right) \left(\frac{v_{\text{apo,f}}}{170 \text{ km s}^{-1}} \right)^2 \left(\frac{v_{\text{th}}}{18 \text{ km s}^{-1}} \right)^{-3} \\ &\sim 700 M_\odot \left(\frac{m_*}{1 M_\odot} \right) \left(\frac{v_{\text{enc}}}{670 \text{ km s}^{-1}} \right) \left(\frac{v_{\text{apo,f}}}{170 \text{ km s}^{-1}} \right)^2 \left(\frac{v_{\text{th}}}{18 \text{ km s}^{-1}} \right)^{-3}. \end{aligned}$$

In the numerical evaluation above, we have normalized v_{th} to the isothermal sound speed for ionized hydrogen at $T = 2 \times 10^4 \text{ K}$. The exact ionized gas temperature depends on gas metallicity (higher metallicity leads to more effective cooling) and on the typical energies of ionizing photons (softer spectra generate lower temperatures). We choose two reference encounter velocities. First, $v_{\text{enc}} = 300 \text{ km s}^{-1}$ is the difference between $(4/3)v_{\text{apo,f}}$ and the velocity of a star also reaching apocenter at r_{apo} but having an eccentricity of 0.4, consistent with the average eccentricity of massive ring stars, which is observed to be¹⁵ $\sim 0.3\text{--}0.4$. Near (but not exactly at) both star's apocenters, a favorably oriented encounter could have this velocity and reduce the angular momentum of the star by approximately the amount estimated above. Second, a perturber from an isotropic population would typically have $v_{\text{enc}} \sim (GM_{\text{BH}}/r_{\text{apo}})^{1/2} = 670 \text{ km s}^{-1}$. From equation (S2), a member of the stellar population of the young ring could serve as the final perturber for a star with mass $m_* \lesssim 0.3 M_\odot$, given a favorable, but not implausible, encounter geometry. A solar mass star likely requires an encounter with a more massive perturber, perhaps an intermediate mass black hole with mass $M_{\text{IMBH}} \sim 10^3 M_\odot$ residing outside of the young disk. Such black holes may be present in the Galactic centre, and are not violating existing dynamical constraints.¹⁸ In fact, Merritt et al. (2009)²⁴ showed that the orbits of the S-stars could be a natural consequence of the interaction between the nuclear star cluster and an intermediate mass black hole (IMBH) with a mass $\gtrsim 1.5 \times 10^3 M_\odot$ on a mildly eccentric orbit over a period of a few Myr. Again, equation (S2) is not a strict requirement for our model, but if it is not satisfied, \dot{M}_w is reduced.

Having established that a final strong encounter can cause a disk-laden star to plunge

toward the black hole without stripping the disk, we now consider the probability of such a history for a star in the Galactic centre. We calculate the rate of delivery of low mass stars onto highly eccentric orbits, the probability of a final encounter that substantially changes the star’s pericenter distance, and the likelihood that a star could be delivered onto a plunging orbit without experiencing a disk-stripping encounter during its lifetime. We make choices about the mass function of stars in the region that are simultaneously optimistic for our theory and consistent with observations.

First, what is the rate of delivery of low-mass stars onto highly eccentric orbits? Over its lifetime T , each low-mass star is scattered multiple times by ring stars of mass m_{pert} at impact parameters $b > b_{\min}$, where b_{\min} is the typical minimum encounter distance after an elapsed time T . The value of b_{\min} is set by the encounter rate $f_{\text{pert}}(b) = [N_{\text{pert}}/(\zeta \pi R^2 h)] \pi b^2 v_{\text{rel}}$, such that $f_{\text{pert}} T = 1$ for $b = b_{\min}$. To avoid disk disruption, b_{\min} must be large enough that disk disrupting encounters are not common. We quantify this constraint below. Here, N_{pert} is the number of perturbing ring stars, v_{rel} is the typical relative velocity between perturbers and the low-mass star, $R = r_{\text{apo}} = 8400 \text{ AU}$ is the local ring radius, $h \sim \sigma_* / \Omega$ is the ring scale height (with $h/R \sim 10^\circ$),¹⁵ σ_* is the velocity dispersion of ring stars, and $\Omega = (GM_{\text{BH}}/R^3)^{1/2}$ is the angular orbital velocity of the ring. We include an order unity factor, ζ , to more accurately approximate the number density of perturbers. We will show below that $\zeta \sim 5$ given our fiducial choices for N_{pert} and R . The measured velocity dispersion $\sigma_* = h\Omega = 120 \text{ km s}^{-1}$ corresponds to expected eccentricities of $\sqrt{2}\sigma_*/(R\Omega) = 0.25$, in rough agreement with observed eccentricities of $e_* = 0.3 - 0.4$. As a compromise between these measured values, we define a stellar random velocity $v_{\text{rand}} = \sqrt{3}\sigma_* \sim e_* R \Omega = 200 \text{ km s}^{-1}$, and we set the typical relative rencounter velocity $v_{\text{rel}} = v_{\text{rand}}$ during the low-mass star’s early orbital evolution, where we have plugged in $e_* = 0.3$. Once the star has reached a highly eccentric orbit, $v_{\text{rel}} \sim \Omega R - v_{\text{apo}} > \sigma_*$ near apocenter, and we adopt $v_{\text{rel}} = \Omega R$.

Diffusion of angular momentum. Transport of stars onto low angular momentum

orbits proceeds by angular momentum diffusion, as in standard loss cone calculations.²⁵ At early times, the impact parameter, b_{strong} , required to generate a “strong” scattering that alters the star’s random velocity by of order itself is $b_{\text{strong}} = Gm_{\text{pert}}/v_{\text{rand}}^2$, and each such scattering generates a fractional angular momentum change of order $v_{\text{rand}}/(\Omega R)$. More generally, as long as $b \geq b_{\min} \geq b_{\text{strong}}$, each star’s specific angular momentum, $J \approx Rv_{\text{apo}}$, is altered by of order itself on a timescale $T_{\text{diff}} = J^2/D$, where the diffusion coefficient

$$\begin{aligned} D &\sim R^2 v_{\text{apo}}^2 \frac{N_{\text{pert}}}{\zeta \pi R^2 h} \pi \left(\frac{Gm_{\text{pert}}}{v_{\text{apo}} v_{\text{rel}}} \right)^2 v_{\text{rel}} \ln \Lambda \\ &\sim \frac{N_{\text{pert}}}{\zeta h} \frac{G^2 m_{\text{pert}}^2}{v_{\text{rel}}} \ln \Lambda \\ &\sim J_c^2 \Omega \frac{N_{\text{pert}}}{\zeta} \ln \Lambda \left(\frac{m_{\text{pert}}}{M_{\text{BH}}} \right)^2 \frac{(\Omega R)^2}{\sigma_* v_{\text{rel}}}, \end{aligned} \quad (S3)$$

where $J_c = R^2 \Omega$ is the specific angular momentum of a star on a circular orbit at the ring radius R , and $\ln \Lambda \equiv \ln(0.08 \text{ pc}/b_{\min})$ is the Coulomb logarithm due to multiple gentle scatterings. Though the diffusion time for stars with angular momentum $J \ll J_c$ is shorter than the relaxation time $T_{\text{rel}} \equiv J_c^2/D$, by a factor²⁵ of $(J/J_c)^2$, the fraction of phase space occupied by low angular momentum orbits is also proportional to $(J/J_c)^2$, so that a population of N_* low-mass stars in the the young stellar ring produces low angular momentum stars a rate²⁶

$$\begin{aligned} f &\sim \frac{N_*}{T_{\text{rel}}} \\ &\sim \Omega N_* \frac{N_{\text{pert}}}{\zeta} \ln \Lambda \left(\frac{m_{\text{pert}}}{M_{\text{BH}}} \right)^2 \frac{(\Omega R)^2}{\sigma_* v_{\text{rel}}}, \end{aligned} \quad (S4)$$

as long as the system is sufficiently relaxed. We return to the question of relaxation below. At early times, $v_{\text{rel}} \sim v_{\text{rand}}$, and at late times $v_{\text{rel}} \sim R\Omega$. However, we note that at late times, the number of perturbers available with comparable relative velocities could easily be a factor of $R\Omega/v_{\text{rand}} \sim 3$ higher given contributions from stellar remnants in the isotropic population, so in estimating our rates, we employ $v_{\text{rel}} = v_{\text{rand}}$. We note that though it plunges interior to the ring’s extent as it approaches pericenter, the cloud nevertheless spends more than half of its orbital time within the ring (near apocenter). As demonstrated above,

disk survival requires $\Delta v_{\text{tid}} \lesssim v_{\text{th}}$, which translates to $b_{\min} \gtrsim [8G^2 m_{\text{pert}} m_*/(v_{\text{enc}} v_{\text{th}}^3)]^{1/2}$. For $m_{\text{pert}} = 60M_{\odot}$, $v_{\text{enc}} = 200 \text{ km s}^{-1}$, and $m_* = 0.3M_{\odot}$, disk survival requires $b_{\min} > 10 \text{ AU}$. At the limit $b_{\min} = 10 \text{ AU}$, $\ln \Lambda \approx 7$. Since $f \propto N_{\text{pert}} m_{\text{pert}}^2$, high-mass stars dominate the stellar orbital evolution.

Mass function of scatterers. For the top-heavy mass function of stars inferred in the young stellar ring,²⁷ the number of stars N having mass m follows $dN/dm \propto m^{-0.45 \pm 0.3}$ in the mass range $7M_{\odot} < m < 60M_{\odot}$, and the presence of higher-mass stars is not excluded. Most of the ring’s mass is associated with the highest mass perturbers, since $m^2 dN/dm \propto m^{1.55}$. The inferred total mass in the young stellar ring of^{15,27} $\sim 10^4 M_{\odot}$ could accommodate $N \sim 170$ perturbers with a mass $m_{\text{pert}} = 60M_{\odot}$ each. The surface density of observed O/WR stars scales radially as²⁷ $\propto r^{-1.4}$, extending from $0.8'' = 0.03 \text{ pc} = 6700 \text{ AU}$ to $12'' = 0.5 \text{ pc} = 10^5 \text{ AU}$ (using a distance to the Galactic centre of $R_0 = 8.33 \text{ kpc}$). Approximately $(1/10)^{0.6} \approx 1/4$ of the ring’s O/WR stars reside at the inner scale of the ring near $r_{\text{apo}} = 1'' \approx 0.04 \text{ pc}$, the location of the proposed initial stellar orbit. Hence, we adopt fiducial values of $m_{\text{pert}} = 60M_{\odot}$ and $N_{\text{pert}} = 40$ in the vicinity of the cloud’s r_{apo} . Integrating over the full disk (with surface density $\Sigma_{\text{pert}}(r)$), we find that $N_{\text{pert}} = 40$ perturbers lie between $R_1 = 6700 \text{ AU}$ and $R_2 = 2 \times 10^4 \text{ AU}$. The volumetric number density of perturbers at $R = 8400 \text{ AU}$ is approximately $\Sigma_{\text{pert}}/(2h) = N_{\text{pert}}/(\zeta \pi R^2 h)$ with $\zeta = (20/3)(R_2^{0.6} - R_1^{0.6})/R_2^{0.6} = 5$.

In contrast, the mass function of observed stars both interior and exterior to the young stellar ring is consistent with a Salpeter/Kroupa initial mass function (IMF).²⁷ We suppose for the sake of argument that the IMF in the young ring changes its slope to the Salpeter value, $dN/dm \sim m^{-2.35}$ below a stellar mass $m < m_{\text{break}} = 7M_{\odot}$ and that this mass function extends down to stars of $0.3M_{\odot}$, consistent with the observed turnover in the IMF in other galactic environments²⁸ (but see also²⁹). Given these assumptions, $N \propto m^{0.55}$ for $m > m_{\text{break}}$ and $N \propto m^{-1.35}$ for $m < m_{\text{break}}$. Then, the inner ring would host ~ 12 stars of $m = 7M_{\odot}$, $N = 170$ stars of $m = 1M_{\odot}$, and $N = 900$ stars of $m = 0.3M_{\odot}$. The presence

of a few thousand young low-mass stars in the ring is consistent with limits from X-ray observations.³⁰ These choices generate delivery rates of $f = 6 \times 10^{-7} \text{ yr}^{-1}$ for $m_* = M_\odot$ and $3 \times 10^{-6} \text{ yr}^{-1}$ for $m_* = 0.3M_\odot$. Scattering on binary stars further enhances our calculated rate.

N-body simulations. However, we must worry about the rate calculation in equation (S4) because the young stellar ring is not relaxed.²⁵ The angular momentum relaxation time $T_{\text{rel}} \sim 3 \times 10^8 \text{ yr}$, and we are interested in timescales more than an order of magnitude shorter than this. We perform a set of N-body simulations using the Mercury6 hybrid orbital integrator³¹ with a timestep of 10 years and accuracy parameter of 10^{-12} . Supplementary Figures S1 and S2 show results from a simulation with 40 fully massive perturbers, each with $m_* = 60M_\odot$, and 900 test particles. Both populations are distributed in semi-major axis from 6700AU to 20100AU with surface densities in semi-major axis proportional to $r^{-1.4}$, consistent with the entire observed disk (not just the simulated inner part) having mass $10^4 M_\odot$. Each particle starts with an eccentricity and inclination randomly drawn from uniform distributions between 0 and 0.3 and between 0 and 10° , respectively. The orbital nodes, arguments of pericenter, and mean anomalies are drawn from a uniform distribution between 0 and 2π . In this simulation, 6 test particles (low mass stars) are delivered to orbits with pericenters less than or equal to that of the infalling cloud between 4 and 6 Myr. The massive perturbers are only mildly excited from their initial disk configuration. In additional simulations (not shown) starting with lower eccentricities and inclinations, the perturbers self-excite to values comparable to those observed on our timescale of interest. The number of stars delivered before 6 Myr onto orbits with pericenter distances less than $r_p = 270 \text{ AU}$ varies substantially from simulation to simulation and can include 0. To elucidate the orbital evolution of the stars, we perform a longer simulation, this time with 24 perturbers having $m_* = 100M_\odot$ and 940 test particles. The results are presented in Supplementary Figure S3. At early times, the distribution of angular momenta

is well matched by a 1-D diffusion equation, with the number plotted

$$N \left(\log_{10} \frac{J}{J_c} \right) = (4\pi Dt)^{-1/2} e^{-(J-J_c)^2/(4Dt)} J \ln(10) N_* \Delta , \quad (S5)$$

where Δ is the binsize. To calculate D , we use equation (S3) with $R = 10^4 \text{AU}$, $h/R = 10^\circ$, $\zeta = \pi$ and $\ln \Lambda = 7$. At late times, phase space fills and $N = N_*(J/J_c)^2 \Delta$, as expected. At 6 Myr, the transition between these regimes is marginal, and small number statistics generate a large variation in outcomes given our fiducial parameters.

The expected closest approach distance, b_{\min} , and the rate of orbital evolution, f , are related by $f \sim T^{-1} p N_* (b_{\text{strong}}/b_{\min})^2 \ln \Lambda$, where $p = v_{\text{rand}}^2 / (\Omega R)^2 = e_*^2$. Rearranging, $b_{\min} \sim b_{\text{strong}} (p N_* / N_{\text{del}})^{1/2} (\ln \Lambda)^{1/2}$, where $N_{\text{del}} \equiv f T$ is approximately the number of stars delivered onto plunging orbits over the age of the system, T . For simplicity, we set $\ln \Lambda = 7$ since variations in b_{\min} considered here will not substantially alter this value. These choices give $b_{\min} \sim b_{\text{strong}}$ if all stars are delivered onto plunging orbits over the system age T and b_{\min} is larger if only a fraction of the population is delivered. Disk disruption is avoided if the delivery fraction $N_{\text{del}}/N_* < (1/8)(\ln \Lambda)(m_{\text{pert}}/m_*)v_{\text{th}}^3/(v_{\text{rand}}\Omega^2 R^2) = 0.01(m_{\text{pert}}/60M_\odot)(0.3M_\odot/m_*)$, where we have chosen to use the expression for early times since low velocity encounters are more disruptive. For reference, in the simulation shown in Supplementary Figure S2, 2/6 of the stars delivered onto plunging orbits at ages between 4 and 6 Myr do not experience disruptive encounters.

Hence, $N_*/300 = 0.5$ solar-mass stars and about $N_*/100 = 10$ stars with $m_* = 0.3M_\odot$ can be delivered over the disk lifetime T without expecting a disk disrupting encounter. For $T = 6$ Myr, the rate f above generates delivery of about $N_*/50$ of each stellar population, for a total of 3 solar mass stars and 20 $0.3M_\odot$ stars. These numbers are comparable within the errors in our calculation, and disks can be safe from disruption.

Other scatterers. What about disruption from encounters with lower-mass stars or with high mass perturbers in an isotropic population? The rate of encounters generating a fixed impulse Δv to the disk scales as $N_{\text{pert}} m_{\text{pert}}^2 / (\sigma_* v_{\text{rel}})$ for a fixed stellar mass. In a given

dynamical population, high mass stars dominate disk disruption, so we need not worry about encounters with low-mass stars in the young disk. For an isotropic population, $(\sigma_\star v_{\text{rel}})^{-1}$ is approximately 0.13 times that for the disk population, so both the star's orbital evolution rate f and the disk disruption rate scale as $0.13N_{\text{pert}}m_{\text{pert}}^2$. Dynamical limits constrain the mass of stars and stellar remnants in the galaxy's central 0.1 pc to be $\lesssim 10^5 M_\odot$.¹⁵ The expected number of low-mass stars and stellar to intermediate mass black holes in this region is not clear.¹⁸ The diffusion of lighter stars out of the ring may have led to the unusually top-heavy mass function of stars that are found in the ring at present,^{15,27,32} and more generally, the isotropic distribution likely contains the remnants of older star formation episodes. For example, $10^5 1M_\odot$ perturbers in an isotropic population would disrupt disks at $\sim 1/10$ the rate of our fiducial $60M_\odot$ perturbers. A large population of intermediate-mass black holes, in contrast, could generate higher disk disruption rates, but the number of such objects, if they exist, is unconstrained and need not be high enough to cause problems for our scenario.

Finally, we return to the probability of a final strong encounter that altered the plunging star's pericenter distance from $2r_p$ to r_p . The ratio of scattering events at b_{\min} to weak scatterings is $1/(\ln \Lambda)$, so about 1/7 injected stars will come in with a strong (i.e., $b \sim b_{\min}$) final scattering event. The rate of orbital evolution due to “ideal” strong scatterings with a favorable encounter velocity due to the encounter geometry is increased relative to the rate of typical strong scatterings by the ratio of the typical to the favorable encounter velocity (gravitational focusing triumphs) and is decreased by the fraction of time spent by a perturber with a favorable velocity. How likely strong scatterings are to occur at favorable encounter velocities depends on the details of the distribution of perturbers, but since we prefer encounters near perturbers' apocenters, where they spend the most time, favorable encounter geometries are not rare.

If one IMBH having mass $M_{\text{IMBH}} = 1.5 \times 10^3 M_\odot$ resides in the central $R = 0.04$ pc of the galaxy, then the likelihood of a strong encounter at $b_{\text{strong}} = GM_{\text{IMBH}}/\sigma_\star^2 = 3\text{AU}$ with

an isotropic $\sigma_* \approx 670 \text{ km s}^{-1}$, capable of sending a star plunging directly from a circular orbit, is approximately $1/(4\pi R^3/3)\pi b_{\text{strong}}^2 \sigma_* T = 0.01$ per star for $T = 6 \times 10^6$ years. This corresponds to 9 injections over the disk lifetime for $N_* = 900$. Stellar encounters with an IMBH at 3AU generate substantial disk stripping. The probability per star of a maximal non-stripping encounter with the IMBH approaches 1, and each such encounter can generate $\Delta v_* \sim 150(0.3M_\odot/m_*)^{1/2} \text{ km s}^{-1}$. One or more IMBHs in the central region could substantially increase the rate of diffusion of low mass stars onto low angular momentum orbits.

Summary. In conclusion, approximately 1/100 of the population of low-mass stars in the young stellar ring could have been delivered by the observed population of $60 M_\odot$ perturbers onto orbits comparable to that of the observed plunging cloud over the age of the young ring without disk stripping. A few thousand young low-mass stars could be present in the ring, consistent with limits from X-ray observations,³⁰ of which about a quarter likely lie in the inner ring. These constraints allow approximately 2×10^{-6} injections of undisrupted disks per year. We conclude that a tail population of low-mass (previously unobserved) stars could diffuse into orbits similar to that of the gas cloud around SgrA*. Is this delivery rate sufficient? A disk orbiting a $0.3M_\odot$ star must have a pericenter distance approximately 2–3 times larger than that of the current cloud in order to remain undisrupted at d_{esc} . On such an orbit, the disk will remain bound indefinitely, and the wind will be regenerated over each orbital period, making the probability of observing such an object in the Galactic centre close to unity. Our calculations are sufficiently approximate that the infalling cloud may represent a long-lived, tidally truncated disk with a continually regenerated wind. If, on the other hand, we need a final kick that recently reduced the pericenter distance of the cloud by a factor of two, that kick needed to generate $\Delta J/J = 1/4$, as calculated above. Such final strong kicks will occur at approximately 16/7 of the delivery rate, where the factor of 16 comes from $(J/\Delta J)^2$ and the factor of 7 comes from the Coulomb log. Over the 140 year period of the cloud, the probability that an infalling disk reaches the current cloud pericenter for the first time is $\sim 0.1\%$. If the cloud is indeed on its first plunge after a

pericenter modification of a factor of two, we are somewhat fortunate to observe it.

Our calculated probability is high enough that observing a plunging young star hosting a proto-planetary disk is plausible. We do not argue that the presence of such an object is likely *a priori*, but rather than the observed young cloud has properties that can be naturally explained given our scenario, and furthermore, our model generates predictions about the future evolution of the cloud that are not common to the pressure-confined cloud model proposed by the discovery team.¹ If our scenario is correct, photoevaporating proto-planetary disks with pericenter distances 2–3 times that of the infalling cloud should be common.

We note that if our suggestion is correct and observations over the next few years confirm that the infalling gas cloud arises from the tidal evolution of a wind blowing off a circumstellar disk, more exotic sources for such a disk need not be considered. For example, a grazing collision between a star and a stellar mass black hole could both put the star onto a sufficiently eccentric orbit and generate debris, a small fraction of which might settle into a disk around the star.³³ However, we consider such a history less natural than our interpretation of the infalling cloud as a young proto-planetary disk.

Other similar systems. Several previous observations in the region of the Galactic centre might also be attributable to proto-planetary disks. Clenet et al. found a flaring infrared source in the L' band at a projected separation of $\sim 0.003\text{pc} = 670\text{ AU}$ from SgrA*.³⁴ The emission is not likely to be stellar since no K -band counterpart was detected (implying $(K - L') > 3$) and the source appears extended. If the emission is associated with dust, it corresponds to a dust temperature of $\sim 10^3\text{K}$ with a total luminosity of $\sim 10L_\odot$. It is possible that this source is of similar origin to the observed infalling cloud considered here, for which K_s , L' , and M band fluxes imply emission from¹ dust with a temperature of $550 \pm 90\text{K}$ and a total luminosity of $\sim 5L_\odot$.

Fritz et al. found that 9 out of 15 objects detected in the K_s and H -bands in the star complex IRS 13E ($\sim 0.14\text{pc} = 3 \times 10^4\text{ AU}$ from SgrA*, with a core radius of about 2500AU)

are very red, consistent with them being warm dust clumps.³⁵ In principle, these dust clumps could be formed by the evaporation of proto-planetary disks around young stars in this complex.

Finally, Muzic et al. reported another star complex IRS 13N at a similar projected separation from SgrA*.³⁶ This complex has a radius of \sim 2000 AU and includes extremely red sources with colors of either dust-embedded stars older than a few Myr or extremely young stars with ages \lesssim 1 Myr. The latter interpretation is supported by the fact that six of the sources are close in projection and show very similar proper motion whose coherence is not expected to survive over an orbital time. Such young stellar objects could naturally host proto-planetary disks of the type required to explain the infalling cloud considered here.

Compact star clusters such as IRS 13N (or IRS 13E), with mass estimates of a few thousand solar masses, could also serve as massive perturbers able to scatter a low-mass star onto the orbit of the plunging cloud.

Supplementary References

23.Jackson, J.M. *et al.*, Neutral Gas in the Central 2 Parsecs of the Galaxy, *Astrophys. J.* **402**, 173-184 (1993).

24.Merritt, D., Gualandris, A. & Mikkola, S., Explaining the Orbits of the Galactic Center S-Stars, *Astrophys. J.* **693**, L35-L38 (2009).

25.Merritt, D., & Wang, J., Loss Cone Refilling Rates in Galactic Nuclei, *Astrophys. J.* **621**, L101-L104 (2005).

26.Wang, J. & Merritt, D., Revised Rates of Stellar Disruption in Galactic Nuclei, *Astrophys. J.* **600**, 149-161 (2004).

27.Bartko, H. *et al.*, An Extremely Top-Heavy Initial Mass Function in the Galactic Center Stellar Disks, *Astrophys. J.* **708**, 834-840 (2010).

28.Bastian, N., Covey, K.R., & Meyer, M.R., A Universal Stellar Initial Mass Function? A Critical Look at Variations, *Annu. Rev. Astro. Astrophys.* **48**, 339-389 (2010).

29.Bonnell, I. A., & Rice, W. K. M., Star Formation Around Supermassive Black Holes, *Science* **321**, 1060 (2010).

30.Nayakshin, S. & Sunyaev, R., The ‘missing’ young stellar objects in the central parsec of the Galaxy: evidence for star formation in a massive accretion disc and a top heavy initial mass function, *Mon. Not. R. Astron. Soc.* **364**, L23-L27 (2005).

31.Chambers, J.E., A hybrid symplectic integrator that permits close encounters between massive bodies, *Mon. Not. R. Astron. Soc.* **304**, 793-799 (1999).

32.Manness, H. *et al.*, Evidence for a Long-standing Top-heavy Initial Mass Function in the Central Parsec of the Galaxy, *Astrophys. J.* **669**, 1024-1041 (2007).

33.Miralda-Escudé, J., A star disrupted by a stellar black hole as the origin of the cloud falling towards the Galactic center. Preprint at <http://arXiv.org/abs/1202.5496> (2012).

34.Clenet, Y. *et al.*, A dual emission mechanism in Sgr A*/L’?, *Astron. & Astrophys.* **439**, L9-L13 (2005).

35.Fritz, T. K. *et al.*, GC-IRS13E—A Puzzling Association of Three Early-Type Stars, *Astrophys. J.* **721**, 395-411 (2010).

36.Muzic, K. *et al.*, IRS 13N: a new comoving group of sources at the Galactic center, *Astron. & Astrophys.* **482**, 173-178 (2008).